Dye Capped Semiconductor Nanoclusters. Role of Back Electron Transfer in the Photosensitization of SnO_2 Nanocrystallites with Cresyl Violet Aggregates

Di Liu, Richard W. Fessenden, Gordon L. Hug, and Prashant V. Kamat*

Radiation Laboratory, University of Notre Dame, Notre Dame, Indiana 46556

Received: August 30, 1996; In Final Form: November 18, 1996[⊗]

Adsorption of a cationic dye, cresyl violet, on SnO_2 and SiO_2 nanoclusters and nanocrystalline thin films results in the formation of H-aggregates. These dyes are photochemically and electrochemically active and extend the photoresponse of large bandgap semiconductors such as SnO_2. Photocurrent generation in dye capped nanocrystalline films of SnO_2 has been demonstrated with visible light excitation. A photon-to-photocurrent generation efficiency around 1% has been observed at 510 nm. Back electron transfer between the photoinjected electron and the oxidized sensitizer plays an important role in controlling the efficiency of net electron transfer. Transient absorption and microwave absorption measurements of the dye aggregate capped SnO_2 films suggest that the back electron transfer is multiexponential and most is completed within a few hundred nanoseconds. The activation energy of the back electron transfer process is very low (∼1.7 kJ/mol).

Introduction

Aggregates of organic dyes play an important role in photosensitization, xerography, and imaging applications.[1−6] Significant interest has been shown in recent years in the study of the photophysical and photochemical behavior of dye aggregates on semiconductor surfaces (see, for example, refs 7−22). Recently, we investigated the excited state behavior of oxazine, squaraine, and rhodamine dye aggregates using transient absorption spectroscopy.[23−27]

Photosensitization is a convenient and useful method to extend the photoresponse of large bandgap semiconductors.[28−32] Cresyl violet has often been used as a model photosensitizer to probe excited state charge transfer at the semiconductor interface. It is interesting to note that the charge injection from excited monomer dye (CV^{+}*) into a semiconductor such as SnS_2 occurs within a few picoseconds.[33−35] Since intersystem crossing is not an efficient process in the monomeric dye, there is no contribution from the triplet excited monomer. On the other hand, intersystem crossing is a feasible route for deactivating a singlet excited aggregate such as $^1(CV)_2^{2+}$*.[36,37] Thus, the triplet excited state becomes a major participant in the charge injection process. Preliminary results related to the picosecond dynamics of cresyl violet aggregates on SnO_2 colloids were reported in our previous study.[26] The rate constant for charge injection from the excited triplet state into semiconductor SnO_2 was determined to be 2×10^8 s^{-1}. The forward and back electron transfer processes which control the photosensitization efficiency of cresyl violet H-aggregates on a SnO_2 nanocluster are illustrated in Scheme 1.

Although the redox couple such as I^{3-}/I^{-} in solution reacts with the oxidized sensitizer, the competing back electron transfer can significantly decrease the efficiency of net electron accumulation within the particles. Therefore the back electron transfer plays a major role in achieving high incident photon-to-photocurrent generation efficiency (IPCE) of photochemical solar cells. For example, the high IPCE observed in the case of ruthenium polypyridyl complex/TiO_2 based photochemical cells has been attributed to the slower back electron transfer process.[38−41] On the other hand, organic sensitizer based photoelectrochemical cells perform very poorly because back electron transfer processes occur at significantly higher rates than the one observed in ruthenium(II) polypyridyl complex/semiconductor systems. In order to assess the role of back electron transfer, we have monitored the fate of the electrons injected into the semiconductor nanocrystallites and their reaction with oxidized sensitizer molecules. The transient absorption and microwave absorption studies which elucidate the role of back electron transfer in cresyl violet aggregate capped SnO_2 nanocrystallites are described here.

SCHEME 1: Charge Injection and Back Electron Transfer in Cresyl Violet H-Aggregate Capped SnO_2 Nanocrystallites[a]

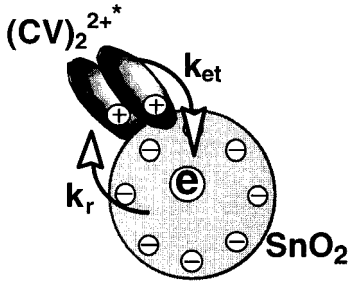

[a] The ratio of forward (k_{et}) and back electron transfer (k_r) rate constants controls the net accumulation of electrons within the semiconductor nanocrystallites. In a photoelectrochemical cell the contribution from k_r is minimized by quickly regenerating the sensitizer with a suitable redox couple.

Experimental Section

Materials. SnO_2 colloidal suspension (18%) was obtained from Alfa Chemicals and used without further purification. SiO_2 colloidal aqueous suspension (14.5%) was obtained from NALCO Chemical Company. The particle diameter of these colloids is in the range 30−50 Å. All the colloidal concentrations indicated in this study are expressed as particle concentrations. (Our estimate of particle concentration is based on the assumption that the colloidal particles are spherical in size with density values of 2.2 and 6.95 g/cm^3 for SiO_2 and SnO_2,

* Address correspondence to this author (e-mail: KAMAT.1@ND.EDU or http://www.nd.edu:80/∼pkamat).

[⊗] Abstract published in *Advance ACS Abstracts,* March 1, 1997.

S1089-5647(96)02695-8 CCC: $14.00

respectively.) Cresyl violet was obtained from Exciton. All other chemicals and solvents were analytical reagents of the highest available purity.

Optically transparent electrodes (OTE) were cut from an indium tin oxide coated glass plate (1.3 mm thick, 20 ohm/square) obtained from Donnelly Corporation, Holland, MI. Absorption spectra were recorded with a Perkin Elmer 3840 diode array spectrophotometer. Unless otherwise specifically indicated, all experiments were performed at room temperature (296 K).

Preparation of SnO_2 and SiO_2 Particulate Films. The synthetic procedure for casting a transparent thin film of SnO_2 on an optically transparent electrode has been reported earlier.[42] A small aliquot (usually 0.1 mL) of the diluted SnO_2 colloidal suspension (0.4%) was applied to a conducting surface of 0.8 $\times$ 3 cm^2 of OTE or a glass slide and was dried in air on a warm plate. The SnO_2 colloid-coated glass plates were then annealed at 673 K for 1 h. The thin film semiconductor electrode is referred to as OTE/SnO_2. A similar procedure was also employed for preparing SiO_2 films on OTE or glass slides. The average thickness as measured from the weight and area of the film was ≤ 1 μm.

Modification with Cresyl Violet Aggregates. We modified the OTE/SnO_2 electrodes with cresyl violet aggregates by dipping the warm OTE/SnO_2 (or SiO_2) electrodes directly in an aqueous solution of cresyl violet for a period of 8−10 h. The electrode was then thoroughly washed with water and stored in the dark. The purple-blue coloration of the porous SnO_2 (or SiO_2) film confirmed capping of cresyl violet H-aggregates on nanocrystallites.[6,25] (These electrodes will be referred to as OTE/SnO_2/$(CV)_2^{2+}$ in the following discussion.)

Photoelectrochemical Measurements. The measurements were carried out in a thin layer cell consisting of a 2 or 5 mm path length quartz cuvette with two side arms attached for inserting reference (Ag/AgCl) and counter (Pt gauze) electrodes. The design of the cell is described elsewhere.[42] A Princeton Applied Research (PAR) Model 173 potentiostat and Model 175 universal programmer were used in the photoelectrochemical measurements. Photocurrent measurements were carried out with a Keithley Model 617 programmable electrometer. A collimated light beam from a 250 W xenon lamp was used as the light source. A Bausch and Lomb high-intensity grating monochromator was introduced into the path of the excitation beam for selecting the excitation wavelength.

Laser-Flash Photolysis Experiments. Nanosecond laser flash photolysis experiments were performed with a Quanta Ray Model DCR-1 Nd:YAG system using a 532 nm (second harmonic) laser pulse ($\sim$6 ns laser width) for excitation.[43] The laser output was suitably attenuated to less than 10 mJ/pulse and defocused to minimize multiphoton processes. Most of the experiments were carried out with low-intensity excitations ($\leq 2 \times 10^{15}$ photons). Under these conditions we expect two to three excited dye aggregate moieties per particle to participate in the charge injection process. The laser flash photolysis of colloidal suspensions was performed in a rectangular quartz cell of 1 cm path length with a right-angle configuration between the direction of laser excitation and analyzing light. The experiments with thin films were carried out in a front-face excitation geometry. The photomultiplier output was digitized with a Tektronix 7912 AD programmable digitizer. A typical experiment consisted of a series of five replicate shots/single measurement. The average signal was processed with an LSI-11 microprocessor interfaced to a VAX computer. A jacketed cell holder which had the provision of thermostat controlled water flow was employed for varying the temperature of the sample.

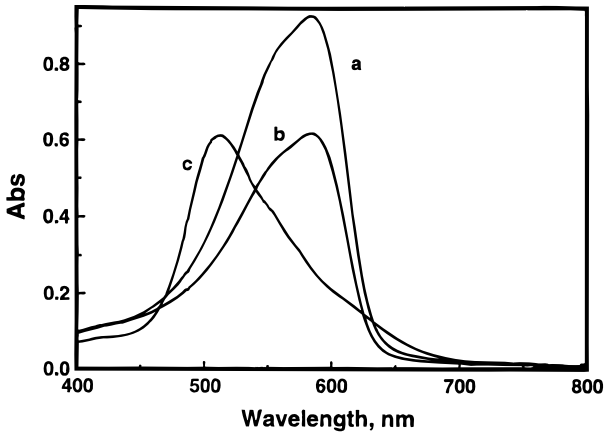

Figure 1. Absorption spectrum of cresyl violet monomer (13 μM) in water: (a) before and (b) after the insertion of OTE/SnO_2 electrode for 12 h. The decrease in the absorbance indicates loss of dye monomer during adsorption on SnO_2 nanocrystallites. Spectrum c shows the absorption spectrum of OTE/SnO_2/$(CV)_2^{2+}$ recorded in air.

Time-Resolved Microwave Absorption Studies. Microwave absorption measurements were made using an apparatus described previously[44] with modifications to improve time response and to allow the phase of the microwave signal to be determined.[45,46] The samples of SnO_2 particle coated fused silica plates (approximately 0.5 $\times$ 1 cm^2) were contained in a fused silica cell. Excitation of the air-equilibrated sample was carried out with a second harmonic laser pulse (532 nm) from a Quanta-Ray Model DCR-1 Nd:YAG laser system (pulse width 6 ns). Relative dose measurements were made by reflecting part of the incident light from a silica plate onto a pyroelectric sensor (Laser Precision Corp. RJP-735).

Results

Aggregation of Cresyl Violet on SiO_2 and SnO_2 Nanocrystallites. In our previous study we have shown that a strong electrostatic interaction between cationic dye, CV^+, and negatively charged SiO_2 or SnO_2 colloids results in the formation of H-aggregates of the dye.[6,25] Similar aggregation could also be seen when the dye from a monomeric solution is adsorbed on thin nanocrystalline films of SnO_2 (or SiO_2). Figure 1 shows absorption spectra (spectra a and b) of the monomeric dye solution before and after immersing the nanocrystalline SnO_2 film. The amount of dye adsorbed on the SnO_2 nanocrystallites corresponds to the decrease in the concentration of the monomeric dye as evidenced from the spectra in Figure 1. The strong electrostatic interaction between the positively charged dye and negatively charged SnO_2 surface yields a monolayer coverage of the dye on the semiconductor surface and thus provides a convenient way to prepare dye capped semiconductor nanoclusters and thin films. It is interesting to note from Figure 1 (spectrum c) that most of the adsorbed dye exists in the aggregate form with a distinctively different absorption band with a maximum at 520 nm. This absorption maximum is blue-shifted as compared to the absorption maximum (585 nm) of the monomer dye, suggesting thereby that the dye aggregate is of the H type (or sandwich geometry). Similar dye aggregation was also observed on SiO_2 colloidal suspensions and thin films. A detailed discussion of cresyl violet aggregation on negatively charged colloid surfaces is reported elsewhere.[24,25] The linear dependence of the absorption at 520 nm on the square of the dye concentration suggests that these dye aggregates consist of dimer units.

Surface-promoted aggregation is not unusual. It has been previously observed in the dimerization of 1,4-anthracence

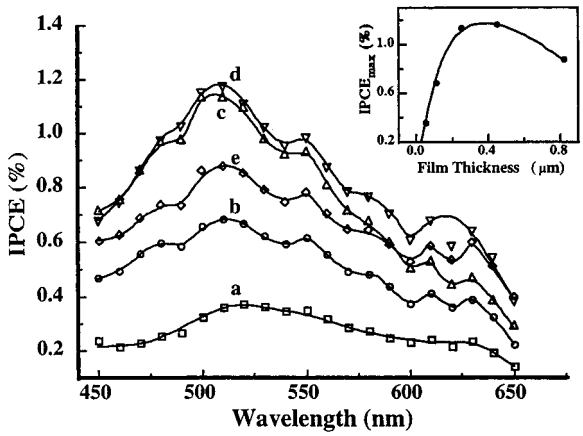

Figure 2. Photocurrent action spectrum of OTE/SnO_2/$(CV)_2^{2+}$ at various SnO_2 film thickness: (a) 0.08, (b) 0.15, (c) 0.23, (d) 0.42, and (e) 0.8 μm. Inset shows the dependence of IPCE at 510 nm on the film thickness. (Electrolyte: 0.5 M KI in water.)

sulfonate on alumina-coated silica[47], rhodamine 6G on SnO_2,[27] and xanthene[48] and cyanine dyes[15,16,49,50] on silica. The appearance of the aggregate absorption band even at very low dye coverages suggests that the distribution of dye molecules on SiO_2 or SnO_2 colloid surface is not random, but that they are bound preferentially to adjacent surface sites.

Photocurrent Generation in SnO_2/$(CV)_2^{2+}$ Films. The dye capped SnO_2 films are electrochemically and photoelectrochemically active. It has been shown earlier[6] that the dye aggregates can be reversibly reduced to yield a colorless dye, and the charges generated can be readily transported through the nanocrystalline semiconductor film. Photocurrent generation could be readily observed when cresyl violet aggregate capped SnO_2 films were used as photoanodes in a photochemical solar cell. The photocurrent action spectra of OTE/SnO_2/$(CV)_2^{2+}$ were recorded by exciting the electrode with monochromatic light. The incident photon-to-photocurrent efficiency (IPCE) as determined from the photocurrent measurements and from expression 1, was evaluated for electrodes with different thicknesses:

$$\text{IPCE (\%)} = 100\,\frac{i_{sc}}{I_{inc}}\,\frac{1240}{\lambda} \qquad (1)$$

where i_{sc} is the short-circuit current (A/cm^2), I_{inc} is the incident light intensity (W/cm^2), and λ is the excitation wavelength (nm). Figure 2 shows the IPCE spectra of OTE/SnO_2/$(CV)_2^{2+}$ at various thicknesses of the SnO_2 film. All these spectra show a maximum around 510 nm which closely matches the absorption maximum of H-aggregates. The close match between the absorption and IPCE maxima suggests that the excited dye aggregates are responsible for the photocurrent generation by injecting electrons into the SnO_2 nanocrystallites. The mechanism of sensitized photocurrent generation is illustrated in Scheme 2. Only a small fraction of the photoinjected electrons are transported toward the collecting surface of OTE to generate a photocurrent while the rest undergo back electron transfer with the oxidized sensitizer.

The observed values of IPCE of ~1% show that most of the incident light is lost without resulting in photocurrent generation. In order to achieve efficient photosensitized current generation at a nanostructured semiconductor electrode, it is essential to meet several important criteria. These include (i) a good match between the energy levels of the oxidation potential of the excited sensitizer and the conduction band of the semiconductor so that the charge injection process is thermodynamically

SCHEME 2: Sensitized Photocurrent Generation in Dye-Capped Nanocrystalline Semiconductor Film

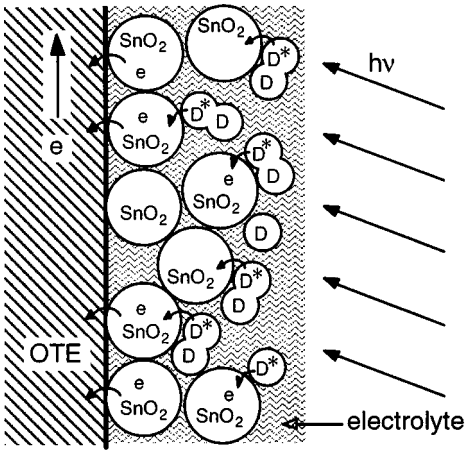

favored, (ii) strong interaction between the sensitizer and the semiconductor, (iii) a broad and intense absorption by the sensitizing dye in the visible, and (iv) a quick regeneration of the sensitizer by reacting with a solution redox couple so that the back electron transfer is kept to a minimum. In the case of the SnO_2/$(CV)_2^{2+}$ system, the first three criteria are readily met. The low values of IPCE observed in the present experiments therefore indicate that the reaction between $(CV)_2^{3+\bullet}$ and I^- from the solution is not very efficient in regenerating the sensitizer and the back electron transfer is a major limiting factor in controlling the net electron transfer.

Figure 2 also shows that an increase in IPCE can be attained by increasing the thickness of the SnO_2 film. However, this dependence on thickness is limited to films of thickness less than 0.4 μm. With increasing thickness we expect an increased amount of dye adsorption on the nanocrystalline SnO_2 film, and as a result, more and more dye molecules participate in the charge injection process to generate a photocurrent. At film thickness $\geq$0.4 μm, all the incident light at 510 nm is absorbed by the sensitizer molecules ($A_{510\ nm} \geq 1$), and therefore, we expect to observe a plateau in the maximum IPCE. However, the photocurrent decreases in thicker films (thickness $\geq$ 0.4 μm). This suggests a significant loss of photogenerated charge carriers during their transit to the collecting surface (OTE). This recombination process at the grain boundaries again highlights the necessity of suppressing back electron transfer to maximize the efficiency of photocurrent generation. The issues related to the charge transport phenomenon in nanocrystalline semiconductor films have been presented in earlier studies.[51−55]

Characterization of Electron Transfer Product, $(CV)_2^{3+\bullet}$ in Nanocrystalline SnO_2 and SiO_2 Films. In our previous study we probed the picosecond dynamics of the charge injection from excited H-aggregates of cresyl violet into SnO_2 colloids.[26] The rate constant for the heterogeneous electron transfer as determined from the transient absorption measurements was 2 $\times$ 10^8 s^{-1}. The transient absorption measurements carried out in the subnanosecond time scale confirmed the participation of triplet excited dye aggregates in the charge injection process. We have now extended the transient absorption study of cresyl violet aggregates on SiO_2 and SnO_2 thin films to probe the photochemical events on the longer time scale, with a particular emphasis on the fate of the electron transfer products, viz., dye aggregate cation radical and injected electron on oxide surfaces.

The transient absorption spectra recorded following 532 nm laser pulse excitation of $(CV)_2^{2+}$ on SiO_2 and SnO_2 thin films are shown in Figures 3 and 4, respectively. Both of these spectra show transient absorption with a maximum at 470 nm which

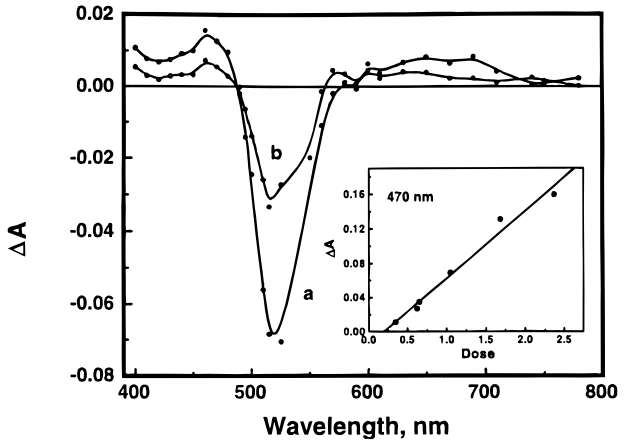

Figure 3. Transient absorption spectra of $(CV)_2^{2+}$ modified SnO_2 film (OTE/SnO_2/$(CV)_2^{2+}$) recorded at (a) 0 and (b) 560 ns after laser pulse excitation. Inset shows the dependence of maximum absorbance of the transient at 470 nm on laser intensity. (Excitation wavelength: 532 nm.)

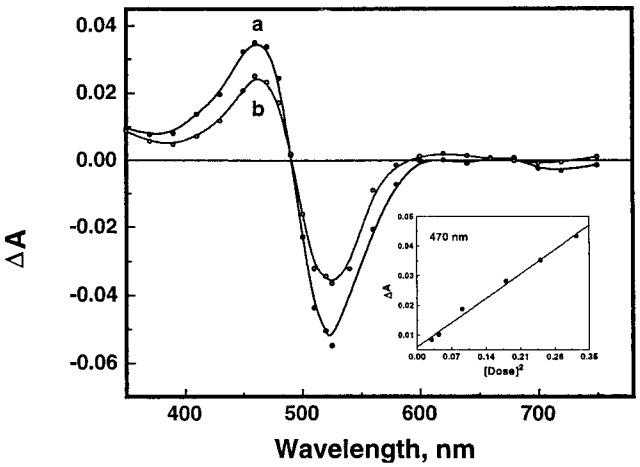

Figure 4. Transient absorption spectra of $(CV)_2^{2+}$ modified SiO_2 film (OTE/SiO_2/$(CV)_2^{2+}$) recorded at (a) 0 and (b) 1.12 μs after laser pulse excitation. Inset shows the dependence of maximum absorbance of the transient at 470 nm on laser intensity. (Excitation wavelength: 532 nm.)

corresponds to the formation of the cation radical, $(CV)_2^{3+\bullet}$. The characterization of this transient has been independently carried out by reacting the dye aggregates with pulse radiolytically generated $^{\bullet}OH$ radicals.[25] As shown earlier,[56,57] an oxide surface can promote the oxidation of the adsorbed sensitizer in two different ways (reactions 2 and 3). In the former case the

$$[SiO_2 \text{ or } SnO_2]\cdots(CV)_2^{2+} + h\nu \rightarrow [SiO_2 \text{ or } SnO_2(e)]\cdots(CV)_2^{3+\bullet} \quad (2)$$

$$[SiO_2 \text{ or } SnO_2]\cdots(CV)_2^{2+} + nh\nu \rightarrow [SiO_2 \text{ or } SnO_2]\cdots((e) + (CV)_2^{3+\bullet}) \quad (3)$$

support material directly participates in the electron transfer process, and in the latter case it promotes excited state ionization of the adsorbed substrate. Both reactions 2 and 3 yield the same products, but the former is a monophotonic process while the latter is a multiphotonic process. In order to distinguish between the two photochemical processes, we determined the dependence of the relative yield of the cation radical, $(CV)_2^{3+\bullet}$, on the excitation laser intensity. The maximum transient absorbance at 470 nm recorded immediately after the laser pulse excitation was used to determine the relative yield of $(CV)_2^{3+\bullet}$. From the

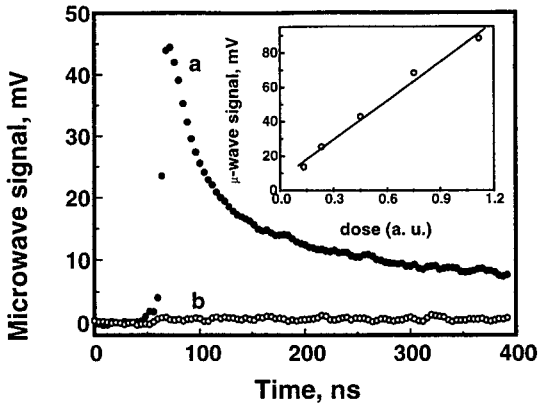

Figure 5. Microwave signal (mV) versus time profiles of (a) SnO_2/$(CV)_2^{2+}$ and (b) SiO_2/$(CV)_2^{2+}$ films under 532 nm laser excitation. The inset shows the dependence of microwave signal of SnO_2/$(CV)_2^{2+}$ on the laser dose.

insets in Figures 3 and 4, it is evident that the production of $(CV)_2^{3+\bullet}$ is proportional to the laser dose on the SnO_2 surface and depends on the square of the laser dose on a SiO_2 surface. This confirms our earlier observation that a monophotonic charge injection process is the dominant process on a semiconducting surface such as SnO_2.[26] On the other hand, a biphotonic photoionization mechanism is operative on the surface of SiO_2. Such a surface promoted multiphoton ionization process has been observed on an oxide surface such as SiO_2 or Al_2O_3.[56,57] SnO_2 is a large bandgap semiconductor with a conduction band around -0.18 V vs NHE at pH 10; while SiO_2 is an insulator with conduction band significantly more negative than the oxidation potential of the excited cresyl violet aggregates. By keeping the laser excitation intensity low, it is possible to promote only the monophotonic charge injection process on a SnO_2 surface.

Back Electron Transfer Process. The photoinjected electrons, if not utilized quickly to generate photocurrent, undergo back electron transfer to regenerate the sensitizer (reaction 4).

$$(CV)_2^{3+\bullet} + SnO_2(e) \rightarrow (CV)_2^{2+} + SnO_2 \quad (4)$$

Both microwave conductivity and transient absorption measurements were carried out to probe the decay of the electron transfer products.

In our previous studies we have demonstrated the usefulness of time-resolved microwave absorption measurements for studying the photosensitization of metal oxide semiconductor particles.[58−60] Visible excitation of the dye-modified semiconductor sample led to an increase in the microwave conductivity of the sample. Since the observed microwave conductivity directly reflects the mobile charge carriers accumulated in SnO_2 nanocrystallites, we would expect its decay to reflect the back electron transfer process. This technique is complementary to measurement of optical absorption by $(CV)_2^{3+\bullet}$ in that the reaction partner is observed.

Typical transient decay profiles of dye aggregate capped nanocrystalline SnO_2 and SiO_2 films are shown in Figure 5. The films were cast on a fused silica plate to facilitate microwave absorption experiments. Excitation of the dye-modified SiO_2 film with a low intensity 532 nm laser pulse does not produce any significant microwave signal. On the other hand, excitation of the dye-modified SnO_2 film with a low intensity 532 nm laser pulse resulted in a prompt appearance of the microwave signal. This indicated that the charge injection process was completed within the laser pulse duration. The dependence of the initial magnitude of the microwave absorption

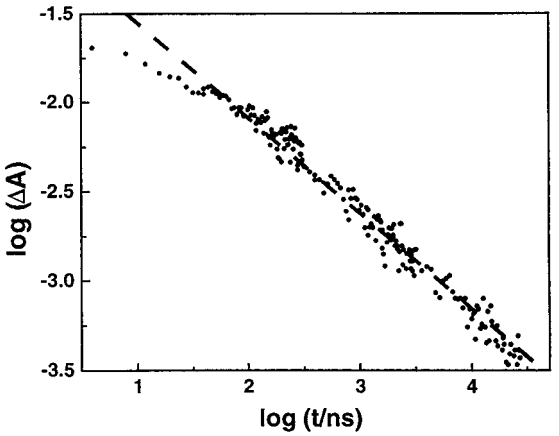

Figure 6. Log−log plot of transient absorbance decay at 470 nm as a function of time (slope = 0.53). The absorption−time profiles of OTE/SnO_2/$(CV)_2^{2+}$ film were recorded over several decades in time following 532 nm laser pulse excitation.

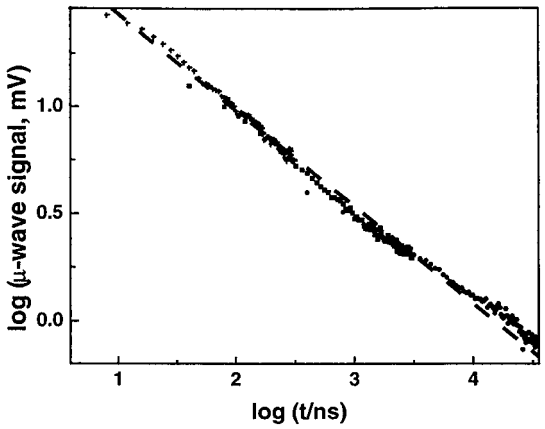

Figure 7. Log−log plot of transient microwave absorption decay as a function of time (slope = 0.46). The microwave absorption−time profiles of OTE/SnO_2/$(CV)_2^{2+}$ film were recorded over several decades in time following 532 nm laser pulse excitation.

on the laser intensity was linear (Figure 5, inset), as one would expect from a monophotonic charge injection behavior. The similarity of this result with that observed in the transient absorption measurements (Figure 3, inset) confirms the complementary nature of these two techniques in probing the charge injection process.

The time dependence of the transient absorption at 470 nm and the microwave absorption recorded over several decades in time are compared in Figures 6 and 7, respectively. It should be noted that these two sets of experiments were carried out with the same sample of nanocrystalline SnO_2 film capped with cresyl violet aggregates. An effort was also made to keep the excitation intensity relatively constant. The decay of these signals is multiexponential as is evident from the log−log plot in Figures 6 and 7. The comparable slopes (∼0.5) of the linear portion of these plots suggests that both techniques are probing same process, the back electron transfer. The multiexponential behavior of the back electron transfer mainly arises from the presence of an inhomogeneous energy distribution of the trapping/detrapping sites at the semiconductor interface.

In order to obtain further information on the kinetics of back electron transfer we analyzed the transient absorption decay of $(CV)^{3+\bullet}$ at 470 nm by fitting it to biexponential decay kinetics. The two rate constants obtained from this analysis give us upper and lower limits for the rate constants with which the back electron transfer occurs. The fast component of the decay was a dominant process contributing 90% or more to the overall

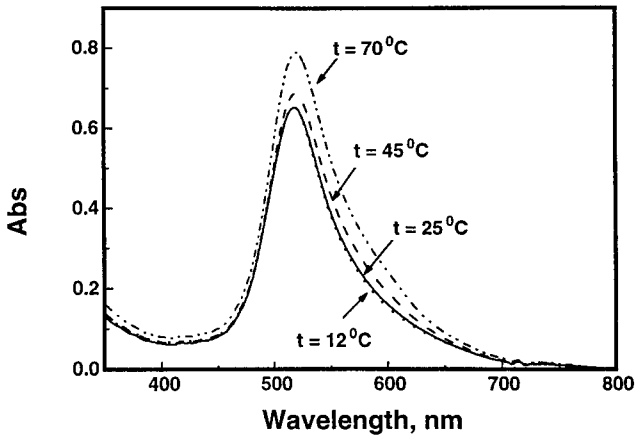

Figure 8. Absorption spectra of 10 μM $(CV)_2^{2+}$ in SnO_2 colloidal suspensions (4.5 μM, pH ∼10) at different temperatures.

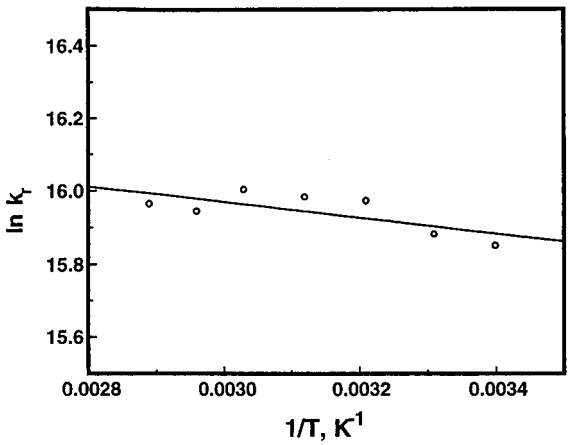

Figure 9. Dependence of log k_r on the inverse of temperature (K^{-1}). Experimental conditions: 10 μM $(CV)_2^{2+}$ in 4.5 μM SnO_2 colloidal suspension (deaerated with N_2). k_r was determined from the fast component of 470 nm transient absorption decay.

decay. This behavior was similar in both colloidal suspensions as well as nanocrystalline thin films. The dependence of the fast decay rate constant on the temperature and excitation intensity has been further investigated in colloidal SnO_2 suspensions (see below).

Temperature Dependence of k_r. The dye aggregates formed on a SnO_2 colloid surface were stable for a wide range of temperatures. No significant changes in the absorption spectra were observed in the temperature range of 285−343 K except for a small increase in the extinction coefficient and a slight broadening at higher temperatures (Figure 8). This allowed us to study the back electron transfer in colloidal SnO_2 suspensions over a wide range of temperatures. The reaction temperature of the jacketed sample cell was varied with thermostat controlled water circulation.

The transient absorption decay at 470 nm was recorded at different temperatures, and the pseudo-first-order rate constant of the fast component k_r was evaluated. The effect of temperature on k_r was marginal. The rate constant increased from 6.6 $\times$ 10^6 to 8.5 $\times$ 10^6 s^{-1} upon increasing the temperature from 285 to 343 K. Figure 9 shows the logarithmic dependence of k_r on the inverse temperature. The activation energy as measured from the Arrhenius plot was very low (E_a =1.7 kJ/mol). Such a low activation energy for a photoinduced electron transfer process on a semiconductor surface is not unusual. Temperature independent heterogeneous charge transfer on semiconductor surfaces has also been reported recently by other researchers.[22,61,62] Such an insensitivity of heterogeneous

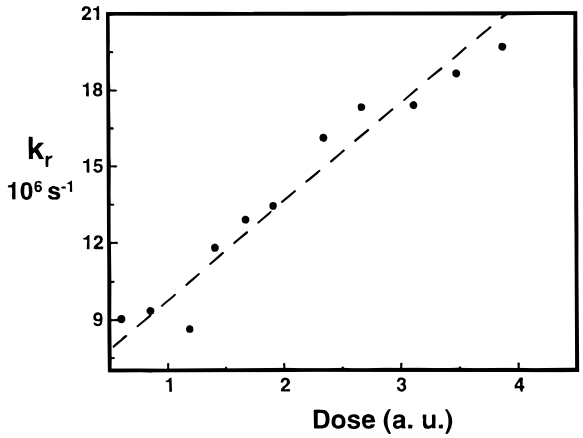

Figure 10. Dependence of k_r on the intensity of excitation laser. k_r was determined from the fast component of 470 nm decay. Experimental conditions: 10 μM $(CV)_2^{2+}$ in 4.5 μM SnO_2 colloidal suspension deaerated with N_2. (The relative laser dose unit of 1 corresponds approximately to 2×10^{15} photons.)

electron transfer to temperature can be explained on the basis of the small reorganization energy of the dye aggregate required for the charge transfer at the semiconductor interface and the strong coupling between the electron donor and acceptor states.

Dependence of k_r on the Excitation Intensity. These experiments were performed with $(CV)^{2+}$ capped SnO_2 colloidal suspensions at different laser pulse excitation intensities. With increasing excitation intensity we expect more of the dye aggregates to participate in the charge injection process, causing an increased accumulation of electrons within the SnO_2 colloidal particle. The decay of cation radicals was monitored at different laser intensities by the procedure described in the previous section, and pseudo-first-order rate constants of the fast component are plotted in Figure 10. The k_r increases from 9×10^6 to 20×10^6 s^{-1} when the laser intensity is increased 4-fold. Although charge separation occurs at the semiconductor interface, higher concentrations of the electron transfer products with increasing laser intensity enhance the observed rate constant, a behavior commonly observed for a bimolecular reaction.

The intensity dependence of the rate constant is consistent with kinetic models of diffusion-controlled processes in spaces that restrict the motion of the reactants. Of particular interest are models that describe the survival probability of pairs of reactants.[63−65] The mathematical model might apply to the current system if the dimer cation is fixed at the south pole of the sphere and the electron diffuses along the surface. The survival probability of such a pair decays exponentially except for multiexponential behavior at short times.[64] A single pair of reactants would correspond to the behavior of the dimers and colloid particles at the lower excitation intensities. At higher excitation intensities additional pairs of reactants would form. However, if the boundary conditions are such that the second radical cation is also in the vicinity of the south pole and the independent pairs approximation [66] is made, then the mean lifetime would decrease by a factor of 2 for a uniform initial distribution of electrons on the surface of the sphere. Boundary conditions with a more realistic distribution of dimer cations could in principle also be analyzed from the Sano and Tachiya model.[63,64] With the model described above, it is possible to understand qualitatively the observed kinetic behavior of an increasingly rapid exponential decay of the dimer cations with increasing excitation intensity.

Discussion

Surface states lying within the bandgap of the semiconductor can play an important role in controlling the interfacial charge transfer at the semiconductor/dye interface.[67] Semiconductor colloids such as SnO_2 possess a large density of surface traps. Metal ion sites such as Sn^{4+} can act as trapping sites for electrons. The photoinjected electrons are quickly trapped at these surface traps. The charge carriers that are trapped near the conduction band edge (or shallow traps) are in equilibrium with the free charge carriers in the conduction band. Under these conditions we can expect both conduction band electrons and trapped electrons to participate in the back electron transfer (reactions 5−7).

$$e_t \leftrightarrow e_{CB} \tag{5}$$

$$e_{CB} + (CV)_2^{3+\bullet} \rightarrow (CV)_2^{2+} \tag{6}$$

$$e_t + (CV)_2^{3+\bullet} \rightarrow (CV)_2^{2+} \tag{7}$$

At low laser intensity the concentration of accumulated electrons in SnO_2 is low. With increasing excitation intensity more and more trap sites get filled. Detrapping of electrons from shallow traps is thermodynamically and kinetically favorable and is a rate-determining step in the back electron transfer. Hence it plays an important role in controlling the kinetics of back electron transfer. On the other hand, the activation energy needed to detrap electrons from deeper traps is significantly higher, and hence their role in the back electron transfer is considered to be negligible. This is also evident from the time-resolved microwave absorption measurements which exhibit temporal behavior similar to that of transient absorption decay. It is likely that either the charge carriers do not have enough time to fall into deeper traps or they are filled within the laser excitation pulse. The time scale with which we monitor the decay of the microwave absorption hence corresponds to the back electron transfer. The influence of trapping and detrapping in the photosensitization behavior of a ruthenium complex adsorbed on an n-type anatase TiO_2 electrode has been shown by Willig and his co-workers.[68] The multiexponential decay of the cation radical which extends up to several hundred nanoseconds suggests the existence of inhomogeneous trap sites.

If the back electron transfer rate is significantly slow, it can facilitate efficient regeneration of the sensitizer by the solution redox couple. This in turn will improve the overall performance of photochemical solar cells. For example, in the case of ruthenium(II) polypyridyl complex and SnO_2, the back electron transfer occurs on the microsecond time scale and is at least 3 orders of magnitude slower than the forward electron transfer (charge injection process). This gives the solution redox couple sufficient time to diffuse through the nanopores and intercept the oxidized sensitizer. These systems with slow back electron transfer therefore show significantly higher power conversion efficiency. On the other hand, organic dye based systems, such as the one employed in the present investigation, show very poor power conversion efficiency. The fast back electron transfer which is only about an order of magnitude smaller than the charge injection rate constant renders net charge transfer less efficient and thus is responsible for the poor photoelectrochemical performance of dye aggregate/semiconductor systems.

In the operation of photoelectrochemical cells, the electrons injected from excited sensitizer molecules into semiconductor nanocrystallites have to be quickly and efficiently transported to the collecting surface of OTE to generate photocurrent. The

SCHEME 3: Transport of Injected Charge across Semiconductor Nanocrystallites[a]

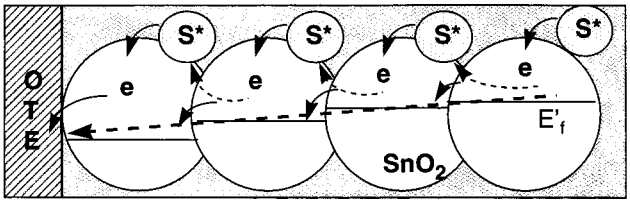

[a] A significant amount of electrons are lost as they recombine with $CV^{3+\bullet}$ at the grain boundaries during their transit to the collecting surface of OTE. E'_f refers to the quasi-Fermi level of the semiconductor nanocluster.

time required for a similarly designed TiO_2 film (thickness 2.7 μm) has been estimated to be $\sim$0.45 μs.[38] Since the back electron transfer between $CV^{3+\bullet}$ and injected electron also occurs on a similar time scale, the reaction with the regenerative redox couple from solution becomes an important step in suppressing the back electron transfer process.

The driving force for the electron transport within the nanocrystalline semiconductor film is created from the varying degree of electron accumulation.[51−55] As more electrons accumulate away from the OTE surface, the quasi-Fermi level is altered in such a way that a potential gradient is created within the thin film (Scheme 3).

Formation of such a potential gradient provides the necessary driving force for the electron transport to the collecting surface of OTE. Since this potential gradient is not an ideal type of Schottky barrier, a significant loss of electrons is encountered during the transit because of their recombination with $CV^{3+\bullet}$ at the grain boundaries. Since more grain boundaries are encountered in thicker films, one would expect greater loss of electrons in the back electron transfer at these grain boundaries. This increased loss of electrons during the transport is evident from the lower IPCE observed with films thicker than 0.4 μm in Figure 2. The measured IPCE in thicker films with excitation from the solution side was also smaller than that obtained with OTE side excitation. Since most of the absorption of incident light in thicker films occurs near the side of excitation, one would expect fewer encounters of grain boundaries when illuminated from the OTE side.

The results described here highlight the necessity of finding new methods to minimize back electron transfer in dye modified semiconductor nanocluster systems so that one can improve the power conversion efficiency of organic dye based solar cells. In order to address this issue, we will focus our future efforts toward the choice of a suitable redox couple that could quickly regenerate the sensitizer, use of multicomponent semiconductor composites for achieving charge rectification, and alteration of the intrinsic properties of semiconductor nanoclusters.

Conclusions

The H-aggregates of cresyl violet are capable of sensitizing large bandgap semiconductors such as SnO_2, but with a very low photon-to-photocurrent efficiency. Back electron transfer has been found to be a major factor controlling the efficiency of net electron transfer. In thicker films (>0.4 μm) recombination at the grain boundaries also plays a major role in decreasing the efficiency of sensitized photocurrent generation. Both the transient absorption and microwave absorption experiments suggest the complexity of the heterogeneous electron transfer at the semiconductor surface.

Acknowledgment. We thank Dr. Simon M. Pimblott for helpful discussions. The work described herein was supported by the Office of Basic Energy Sciences of the U.S. Department of Energy. This is Contribution No. 3960 from the Notre Dame Radiation Laboratory.

References and Notes

(1) Loutfy, R. O.; Law, K.-Y. *J. Phys. Chem.* **1980**, *84*, 2803.
(2) Valdes-Aguilera, O.; Neckers, D. C. *Acc. Chem. Res.* **1989**, *22*, 171.
(3) Law, K. Y. *Chem. Rev.* **1993**, *93*, 449.
(4) Hotchandani, S.; Das, S.; Thomas, K. G.; George, M. V.; Kamat, P. V. *Res. Chem. Intermed.* **1994**, *20*, 927.
(5) Kim, Y.-S.; Liang, K.; Law, K.-Y.; Whitten, D. G. *J. Phys. Chem.* **1994**, *98*, 984.
(6) Liu, D.; Kamat, P. V. *J. Electrochem. Soc.* **1995**, *142*, 835.
(7) Chibisov, A. K.; Slavnova, T. D. *J. Photochem.* **1978**, *8*, 285.
(8) Rentsch, S. K.; Danielius, R. V.; Gadonas, R. A.; Piskarskas, A. *Chem. Phys. Lett.* **1981**, *84*, 446.
(9) Brumbaugh, D. V.; Muenter, A. A.; Knox, W.; Mourou, G.; Wittmershaus, B. *J. Lumin.* **1984**, *31*, 783.
(10) Gerischer, H.; Bressel, B. *Ber. Bunsen-Ges. Phys. Chem.* **1985**, *89*, 1083.
(11) Tanaka, M.; Nakazawa, N.; Tanaka, I.; Yamashita, H. *Chem. Phys.* **1985**, *97*, 457.
(12) Gomes, A. S. L.; Taylor, J. R. *J. Photochem.* **1986**, *32*, 325.
(13) Quitevis, E. L.; Horng, M.-L.; Chen, S.-Y. *J. Phys. Chem.* **1988**, *92*, 256.
(14) Sundstrom, V.; Gillbro, T.; Gadonas, R. A.; Piskarskas, A. *J. Chem. Phys.* **1988**, *89*, 2754.
(15) Chen, S.-Y.; Horng, M.-L.; Quitevis, E. L. *J. Phys. Chem.* **1989**, *93*, 3683.
(16) Horng, M.-L.; Quitevis, E. L. *J. Phys. Chem.* **1989**, *93*, 6198.
(17) Sato, T.; Yonezawa, Y.; Hada, H. *J. Phys. Chem.* **1989**, *93*, 14.
(18) Tani, T.; Suzumoto, T.; Kemnitz, K.; Yoshihara, K. *J. Phys. Chem.* **1992**, *96*, 2778.
(19) Wantanabe, M.; Herren, M.; Morita, M. *J. Lumin.* **1994**, *58*, 198.
(20) Taguchi, T.; Hirayama, S.; Okamoto, M. *Chem. Phys. Lett.* **1994**, *231*, 561.
(21) Khairutdinov, R. F.; Serpone, N. *J. Phys. Chem.* **1995**, *99*, 11952.
(22) Trosken, B.; Willig, F.; Schwarzburg, K. *J. Phys. Chem.* **1995**, *99*, 5152.
(23) Kamat, P. V.; Hotchandani, S.; de Lind, M.; Thomas, K. G.; Das, S.; George, M. V. *J. Chem. Soc., Faraday Trans.* **1993**, *89*, 2397.
(24) Liu, D.; Hug, G. L.; Kamat, P. V. *J. Phys. Chem.* **1995**, *99*, 16768.
(25) Liu, D.; Kamat, P. V. *Langmuir* **1996**, *12*, 2190.
(26) Liu, D.; Kamat, P. V. *J. Chem. Phys.* **1996**, *105*, 965.
(27) Nasr, C.; Liu, D.; Hotchandani, S.; Kamat, P. *J. Phys. Chem.* **1996**, *100*, 11054.
(28) Gerischer, H. *Photochem. Photobiol.* **1972**, *16*, 243.
(29) Gerischer, H.; Willig, F. *Top. Curr. Chem.* **1976**, *61*, 31.
(30) Parkinson, B. A.; Spitler, M. T. *Electrochim. Acta* **1992**, *37*, 943.
(31) Hagfeldt, A.; Grätzel, M. *Chem. Rev.* **1995**, *95*, 49.
(32) Kamat, P. V. In *Molecular level artificial photosynthetic materials.* Progress in Inorganic Chemistry Series; Meyer, J., Ed.; John Wiley & Sons, Inc.: New York, 1997; Vol. 44; p 273.
(33) Eichberger, R.; Willig, F. *Chem. Phys. Lett.* **1990**, *141*, 159.
(34) Willig, F.; Eichberger, R.; Sundaresan, N. S.; Parkinson, B. A. *J. Am. Chem. Soc.* **1990**, *112*, 2702.
(35) Kietzmann, R.; Willig, F.; Weller, H.; Vogel, R.; Nath, D. N.; Eichberger, R.; Liska, P.; Lehnert, J. *Mol. Cryst. Liq. Cryst.* **1991**, *194*, 169.
(36) McRae, E. G.; Kasha, M. *J. Chem. Phys.* **1958**, *28*, 721.
(37) Kasha, M.; Rawls, H. R.; El-Bayoumi, M. A. *Pure Appl. Chem.* **1965**, *11*, 371.
(38) O'Regan, B.; Moser, J.; Anderson, M.; Grätzel, M. *J. Phys. Chem.* **1990**, *94*, 8720.
(39) O'Regan, B.; Grätzel, M. *Nature (London)* **1991**, *353*, 737.
(40) Nazeeruddin, M. K.; Kay, A.; Rodicio, I.; Humphry, B. R.; Mueller, E.; Liska, P.; Vlachopoulos, N.; Grätzel, M. *J. Am. Chem. Soc.* **1993**, *115*, 6382.
(41) Kamat, P. V.; Bedja, I.; Hotchandani, S.; Patterson, L. K. *J. Phys. Chem.* **1996**, *100*, 4900.
(42) Bedja, I.; Hotchandani, S.; Kamat, P. V. *J. Phys. Chem.* **1994**, *98*, 4133.
(43) Nagarajan, V.; Fessenden, R. W. *J. Phys. Chem.* **1985**, *89*, 2330.
(44) Fessenden, R. W.; Carton, P. M.; Shimamori, H.; Scaiano, J. C. *J. Phys. Chem.* **1982**, *86*, 3803.
(45) Fessenden, R. W.; Scaiano, J. C. *Chem. Phys. Lett.* **1985**, *117*, 103.
(46) Fessenden, R. W.; Hitachi, A. *J. Phys. Chem.* **1987**, *91*, 3456.
(47) Ford, W. E.; Kamat, P. V. *J. Phys. Chem.* **1989**, *93*, 6423.
(48) Avnir, D.; Levy, D.; Reisfeld, R. *J. Phys. Chem.* **1984**, *88*, 5956.
(49) Kemnitz, K.; Yoshihara, K.; Ohzeki, K. *J. Phys. Chem.* **1990**, *94*, 3099.
(50) Watanabe, M.; Herren, M.; Morita, M. *J. Lumin.* **1994**, *58*, 198.

(51) Hodes, G.; Howell, I. D. J.; Peter, L. M. *J. Electrochem. Soc.* **1992**, *139*, 3136.
(52) Hodes, G. *Isr. J. Chem.* **1993**, *33*, 95.
(53) Vinodgopal, K.; Hotchandani, S.; Kamat, P. V. *J. Phys. Chem.* **1993**, *97*, 9040.
(54) Hagfeldt, A.; Lindquist, S. E.; Grätzel, M. *Sol. Energy Mater. Sol. Cells* **1994**, *32*, 245.
(55) Nasr, C.; Hotchandani, S.; Kamat, P. V.; Das, S.; George Thomas, K.; George, M. V. *Langmuir* **1995**, *11*, 1777.
(56) Gopidas, K. R.; Kamat, P. V. *J. Phys. Chem.* **1989**, *93*, 6428.
(57) Kamat, P. V. *Chem. Rev.* **1993**, *93*, 267.
(58) Fessenden, R. W.; Kamat, P. V. *Chem. Phys. Lett.* **1986**, *123*, 233.
(59) Bedja, I.; Hotchandani, S.; Carpentier, R.; Fessenden, R. W.; Kamat, P. V. *J. Appl. Phys.* **1994**, *75*, 5444.
(60) Fessenden, R. W.; Kamat, P. V. *J. Phys. Chem.* **1995**, *99*, 12902.
(61) Kietzmann, R.; Ehret, A.; Spitler, M.; Willig, F. *J. Am. Chem. Soc.* **1993**, *115*, 1930.
(62) Moser, J. E.; Grätzel, M. *Chem. Phys.* **1993**, *176*, 493.
(63) Tachiya, M. *Chem. Phys. Lett.* **1980**, *69*, 605.
(64) Sano, H.; Tachiya, M. *J. Chem. Phys.* **1981**, *75*, 2870.
(65) Szabo, A.; Schulten, K.; Schulten, Z. *J. Chem. Phys.* **1980**, *72*, 4350.
(66) Steinberg, I. Z.; Katchalski, J. *J. Chem. Phys.* **1968**, *48*, 2404.
(67) Yamase, T.; Gerischer, H.; Lubke, M.; Pettinger, B. *Ber. Bunsen-Ges. Phys. Chem.* **1978**, *82*, 1041.
(68) Schwarzburg, K.; Willig, F. *Appl. Phys. Lett.* **1991**, *58*, 2520.